Interpretation of shallow electromagnetic instruments resistivity and magnetic susceptibility measurements using rapid 1D/3D inversion

Christophe Benech, Michel Dabas, François Xavier Simon, Alain Tabbagh, Julien Thiesson

Interpretation of shallow EMI resistivity and magnetic susceptibility measurements using rapid 1D/3D inversion

Short title: Rapid1D/3D inversion of shallow EMI

Authors: Christophe Benech[1], Michel Dabas[2], François-Xavier Simon[3], Alain Tabbagh[4], Julien Thiesson[4]

[1] UMR 5133 Archéorient, Maison de l'Orient et de la Méditerranée – Université Lyon 2 F-69365 Lyon

[2] Geocarta, 5 rue de la banque F-75002 Paris

[3] USR3550, MSH, 4 rue Ledru, F-63000, Clermont-Ferrand

[4] Sorbonne Universités, UPMC Paris6, UMR7619, Métis, F-75252 Paris

Corresponding author: Alain Tabbagh, alain.tabbagh@upmc.fr

Abstract

This paper proposes an inversion process of EMI data based on a two-step approach with 1D inversion of the entire studied surface and a fast 3D inversion applied over limited areas. This process is similar to that formerly used in resistivity prospection. For the study of soil (environmental, engineering or archaeological explorations) low frequency electromagnetic instruments (referred to as Slingram EMI, or EMI) have highly useful specificities. They are light, easy to move in the field, and can simultaneously measure the ground's electrical conductivity and magnetic susceptibility; they have thus been used to map these properties over large surface areas, within relatively short periods of time and at reasonable expense. The possibility of combining several coil geometries has opened up the potential for multi-depth techniques and systematic 1D inversion, which are found to be sufficiently revealing to allow larger portions of surveyed areas to be analysed.

In the ‘targeted areas’ selected for 3D inversion, the geometries of the 3D features and the resistivity and/or susceptibility contrasts are determined. This step is based on the method of moments where only 3D heterogeneities are meshed, and only a small number of major characteristics, such as contrast, thickness, width, etc., are searched for. This process was first applied to synthetic data, then to data acquired at an experimental test site, and finally to field cases. The rapid 3D inversion complements the 1D one by solving a series of issues: correction for the apparent anisotropy generated by the instrument configuration, multi-arched anomalies, precise location of lateral changes and determination of the properties contrasts. The inversion results highlight the importance of the instrument geometry. It is also shown that apparent magnetic susceptibility data can be more appropriate for the determination of the volume of man-made features, and is highly complementary to conductivity data.

Key words

Soil resistivity and magnetic susceptibility, multi-depth EMI prospection, 1D and 3D successive inversions, archaeological prospection

Introduction

The application of Slingram electromagnetic induction (EMI) devices to near-surface studies began during the 1960s in archaeological prospection. The data initially gave rise to a series of interpretation difficulties, due to the unexpected influence of the ground's magnetic susceptibility in the measured responses (Scollar et al. 1990). It was later recognized that an appropriate choice of coil separation and frequency could allow the conductivity response to be distinguished from that of the magnetic susceptibility (Tite and Mullins, 1970): in cases where the so-called induction number is sufficiently low, the magnetic susceptibility generates an in-phase response while the electrical conductivity a quadrature out of phase one.

The attractive benefits of this technique have led to considerable research, in an effort to assess its potential advantages and drawbacks with respect to those of the previously implemented, conventional magnetic field and DC resistivity techniques. The design of a new family of EM instruments by Geonics Ltd (Canada) (McNeil 1980) led to large applications in soil salinity mapping (De Jong et al. 1979), which were then extended to the study of other soils (Kachanoski et al. 1988).

Conductivity measurements are straightforward with an EMI instrument, since it can be more easily deployed and operated in the field than a DC resistivity array. EMI instruments have thus experienced considerable developments, for rapid near-surface mapping applications over extended areas (Bendjoudi et al. 2002, Vitharana et al. 2008, Hoefer et al. 2010). Similarly to the case of airborne electromagnetic measurements (AEM) prospectors have to face with the complexity of interpreting huge volumes of 3D data (see for example Huang and Fraser, 1996). The first interpretations involved the application of a 1D point-by-point inversion, after having outlined the conditions under which this interpretation is relevant (Guérin et al. 1996). Later, the development of 1D modelling included magnetic susceptibility and dielectric permittivity in the analysis of EMI data (Huang and Fraser 2002, Farquharson et al. 2003). Similarly to the case of galvanic resistivity, more sophisticated laterally-constrained 1D inversions have been applied (Santos 2004, Auken and Christiansen 2004) or joint inversion has been used with other techniques, magnetic cartography in particular (Benech et al. 2002).

Nowadays, new ground-based multi-coil devices (Saey et al. 2012, Bonsall et al. 2013) give access to precise multi-depth data, while ensuring accurate collocation of the data fields. This stimulates the need of inversion procedures that fully exploit the advantages of these instruments, in terms of imaging both conductivity and susceptibility of subsurface features. One also wants to take into account the need of a rapid method usable on a laptop allowing

easily reconsidering the starting parameters and the extent of the considered area. Compared with other EM techniques one must note that both the transmitter(s) and the receiver(s) are moving thus (i) the considered calculations are significantly longer than for fixed sources EM because the primary field needs to be calculated for each location of the transmitter, but (ii) in the surveyed field the electromagnetic coupling is negligible between 3D heterogeneities separated by too great distances (several times the inter-coil separation(s)). To overcome the difficulties and taking into consideration the practical conditions associated with 3D inversion, a two-steps efficient approach has been proposed for the processing of multi-depth DC resistivity data (Brinon et al. 2012). The first step involves defining the 1D structure of the subsurface. Then the interpreter defines a 'targeted area', which is a limited area surrounding the target(s) of interest and whose surface is several times larger than the range of investigation of the instruments used. The 3D bodies imbedded in the layered terrain are characterized by a limited number of parameters: contrast, thickness, width, length, orientation. This approach is well matched to the characteristics of man-made features that are searched for in archaeological prospection, or in polluted sites exploration. It is straightforwardly implemented when using the moment method (MoM) for forward modelling. MoM combines analytical and numerical calculations, for which only 3D heterogeneities located in a layered 1D terrain need to be meshed. Its application in EM is less simple than in DC resistivity but both the conductivity and susceptibility contrasts can be taken into account (Tabbagh 1985).

In the present paper this approach is applied to EMI survey data in order to evaluate its potential. One first defines the successive steps of the inversion process before inverting synthetic data, data collected above artificial features on a field test site and finally field data collected over archaeological sites.

Inversion process

Forward modelling

The moment method (MoM) has been applied for more than thirty years in EM prospection modelling (Raiche 1974, Hohmann 1975, Tabbagh 1985). 3D bodies located in layered terrain are replaced by an equivalent set of EM dipoles sources. Consequently it allows meshing to be restricted to heterogeneous bodies, but requires an initial 1D layered model and analytical calculations of the fields generated by dipole sources in the layered terrain. These can now be performed very rapidly through the use of convolution calculations to determine the required Hankel transforms (Guptasarma and Singh, 1997). After having determined the 1D surrounding model, the heterogeneous body(ies) imbedded in the layers is (are) meshed, and the intensity of the equivalent secondary sources is determined using a volume integral equation. These sources are then used to compute the resulting secondary field at the surface.

Inversion

The aim of an inversion process is to determine the unknown quantities representing physical properties of interest. In the present case, these correspond to the electrical resistivity and magnetic susceptibility values, and the geometrical boundaries of selected layer(s) and body(ies). The inversion is achieved by starting with an *a priori* set of values, representing each of the different inversion parameters, and then iteratively modifying these in order to achieve a sufficiently good fit between the results of the forward model and the experimental data. The Levenberg-Marquardt algorithm (Marquardt, 1963) is used to achieve a linearized iterative process, in which the cost function includes both the Euclidian distance (L2 norm) between the model results and the data, as well as the intensities of the model parameter increments, multiplied by a damping factor the weight of which is reduced during the course of the iterative process.

In the present case the total inversion process thus follows two steps. The first of these determines, over the entire studied area, an optimised 1D structure that is fitted (point by point, or with a lateral constraint) to the apparent resistivities and susceptibilities measured by the various instruments. In this step, if vertical electrical sounding results are not available, one generally fixes the number of layers at 3 and chooses the *a priori* resistivity and thickness values by considering the apparent resistivity and magnetic susceptibility values as well as the depth of investigation of each EMI configuration used.

The algorithm is the following. We called **m** the vector of the parameters, $\mathbf{m_0}$ the corresponding *a priori* starting values, **d** the vector of the data and **G** the operator of the forward calculation. As the problem is non-linear, it is iteratively solved by calculating at iteration, *i*, **G** and its Jacobian **J** using $\mathbf{m_{i-1}}$ parameters and then deducing the increment $\mathbf{\Delta m=m-m_{i-1}}$ by derivation of the cost function:

$$\mathbf{S=\Delta p^T\Delta p+\lambda\Delta m^T\Delta m} \quad (1)$$

Where

$$\mathbf{\Delta p=d-Gm_{i-1}-.J\Delta m} \quad \mathbf{(2)}$$

The solved equation is thus:

$$\mathbf{J^TJ+\lambda I)\Delta m=J^T\Delta p} \quad \mathbf{(3)}$$

Where **I** is the identity matrix and λ the regularisation parameter. λ has a starting value equal to the double of the trace of the $\mathbf{J^TJ}$ matrix divided by the number of parameters and, after, is divided at each iteration *i* by $i^{1.5}$. The number of iteration depends on the $\mathbf{m_0}$ choice but remains lower than 10.

Where a 3D approach is required, the second step begins by defining, over the 'targeted area' surrounding the body(ies), the 1D reference or 'background' model. We adopt the statistic mode of each value of the layer's parameters in that area. Then the parameters

151 characterising the 3D heterogeneous body(ies) are determined. The *a priori* starting values of
152 the horizontal limits the body(ies) are defined by considering the full width half maximum of
153 the anomaly, that of the resistivity by dividing by two the background resistivity if the body is
154 more conductive and by multiplying by two the background resistivity is the body is more
155 resistive. To verify the influence of these a priori values they can also be freely fixed by the
156 interpreter. In 3D inversion the starting value of regularisation parameter, λ, equals the fifth of
157 the trace of the matrix divided by the number of parameters. The susceptibility contrast is
158 linearly inversed.

159 The electrical resistivity and magnetic susceptibility are nevertheless two independent
160 properties, but whereas the resistivity distribution modifies the 'primary' field distribution
161 seen by the magnetic grains inside the layered terrain (which could be significantly different
162 from the free space distribution), the susceptibility (and the susceptibility contrast) is
163 sufficiently small for its influence on the primary field to be considered as negligible
164 (Tabbagh 1985). This means that the resistivity distribution must be known before the
165 susceptibility distribution can be inverted, whereas the converse does not apply. In both the
166 1D and 3D inversion steps, we thus proceed by initially inverting the resistivity distribution
167 and the geometrical limits, before searching for the susceptibility distribution.

168 ***Tests of rapid 1D/3D inversion on synthetic data***

169 Although the 1D inversion of apparent resistivity data maps is well known and has
170 been used and published for more than twenty years (Guérin *et al*. 1996), the 3D inversion of
171 data raises new issues. The first difficulty, of major importance for the prospector, is to assess
172 the optimal number of independent in-phase and quadrature out of phase measurement maps
173 needed to determine the required resistivity and susceptibility contrasts as well as the
174 geometrical parameters of the body(ies). Although this problem is complex and probably has

175 no general solution, the analysis of a synthetic example can contribute to an improved
176 understanding of this process.

177 We consider a 3D elongated body 3 m in length, 1 m in width and 1 m in thickness
178 (which could correspond to a ditch) embedded in the second layer of a three-layer ground
179 having a resistivity of 20 Ωm (50 mSm^{-1} conductivity) and a susceptibility of 80 x 10^{-5} SI.
180 The top of the body is located 0.3 m below the ground. The first layer (corresponding to the
181 topsoil) has a resistivity of 100 Ωm (10 mSm^{-1}), a susceptibility of 30 x 10^{-5} SI, and a
182 thickness equal to 0.2 m. The second layer is characterised by the same parameters with the
183 values: 200 Ωm (5 mSm^{-1}), 20 x 10^{-5} SI and 2m, and the third layer is characterised by the
184 values: 50 Ωm (20 mSm^{-1}) and 10 x 10^{-5} SI. The synthetic data are calculated for three
185 different Slingram EMI devices: a) a 0.6 m coil separation with HCP (horizontal coplanar)
186 and VCP (vertical coplanar) coil configurations, an operating frequency equal to 27.96 kHz,
187 and measurements recorded at 0.08m above the ground; b) a 1.0 m coil separation with HCP
188 and VCP coil configurations, an operating frequency equal to 14.6 kHz, and measurements
189 recorded at 0.08m above the ground; c) a 1.5 m separation with a PERP (perpendicular) coil
190 configuration, an operating frequency equal to 8 kHz, and measurements recorded 0.15 m
191 above the ground. We thus have ten independent data sets, of which five correspond to in-
192 phase measurements expressed by apparent susceptibility values (Figure 1b) and five
193 correspond to quadrature measurements expressed by apparent resistivity values (Figure 1a),
194 calculated with a fine 0.25 x 0.25 m^2 mesh over a 8 x8 m^2 surface area, corresponding to a
195 total of 1089 measurement points.

196 *1D inversion results*

197 Here the inversion bears over one single unknown parameter, the resistivity
198 (respectively susceptibility of the second layer) in order to be able to compare the results of
199 the different configurations. As expected from theory (Tabbagh 1986), for the apparent

resistivity measurements VCP configurations give the best results, with a full width half maximum corresponding to the width of the body, and a minimum reaching 60 Ωm (16.7 mSm^{-1}) for a 1 m VCP, whereas the latter parameter is determined as 100 Ωm (10 mSm^{-1}) for a 1m HCP configuration, and 97 Ωm (10.3 mSm^{-1}) for the PERP 1.5 m instrument. When the five sets of data are inverted together, the resulting image is less informative than when the VCP configuration is used alone, and the resistivity minimum is determined to be 84 Ωm (11.9 mSm^{-1}). It can thus be understood that it is not necessarily relevant to use several datasets due to its unavoidable 'averaging' effect. However, the difference between the 1D results and the resistivity of the body (20 Ωm) always remains high.

The 1D inversion of apparent susceptibility datasets produces similar results, except that, as in the apparent susceptibility maps (Figure 1b), the shapes of the anomalies fit the shape of the body more accurately. Similarly to the case of the resistivity, the VCP configuration produces the best result: the VCP 1m thus leads to a 55 x 10^{-5} SI maximum, whereas the HCP 1m leads to 45 x 10^{-5}SI, the PERP gives 52 x 10^{-5} SI and all five datasets also find 52 x 10^{-5} SI for the predefined 80 x 10^{-5} SI susceptibility of the body.

3D inversion results

Using the full width half maxima, it is relatively straightforward to determine the shape of the body in the horizontal plane. In the following, we focus on assessing the suitability of various instrument geometries/configurations for the determination of three parameters: the body's vertical extent, its resistivity/conductivity contrast, and its susceptibility contrast. The vertical extent of a body is known to be the most difficult parameter to asses, using the DC resistivity method. The inversion is based on the data corresponding to a small area, i.e. the selected targeted area comprising 5x21 measurement points centred on the body (thus a 1 x 5 m^2 area, Figures1a and 1b). The results obtained with each dataset (corresponding to 5 different instrumental configurations), and with the

combined datasets, are presented in Table 1. These include results based on both apparent resistivity measurements, and apparent susceptibility measurements. It can be seen that the computed results are close to the real values (provided in the first line of this table), with the exception of the vertical extent of the body, determined by inverting the apparent resistivity data, which has uncertainties as high as 20%. The most accurate results, obtained using the apparent susceptibility data, can be explained by the stronger geometrical correspondence between the shape of the anomaly and the shape of the causative body. In this example, the VCP 1m configuration appears to produce the best inversion results. The most inaccurate resistivity inversion is determined with the PERP instrument (probably as a result of its greater 1.5m inter-coil separation), and the most inaccurate susceptibility inversion is determined with the HCP (probably because it has the smallest anomaly). It is important to note that this conclusion is valid even in the case of the smallest inter-coil separation, in agreement with previously published experimental results (Thiesson *et al*. 2009). Again there is no clear advantage in using the five data sets together, two of the one data sets giving better results.

Field test over an artificial feature

A field test over artificial features has several advantages when compared to (physical or numerical) modelling: 1) it makes use of real in-field measurements, associated with the usual errors arising from uncertainties in measurement locations, external sources of EM noise, etc., 2) even when the anomalous bodies are built very carefully, the homogeneity of the filling material is never perfect, thus leading to real variability in the body properties, 3) the surrounding medium may also be inhomogeneous, and be characterised by significant natural changes in the immediate vicinity of the body.

The artificial feature we studied is located at the Garchy laboratory (Nièvre, France). It consists of a dual-branch ditch, dug into a silty superficial weathered formation above the Jurassic limestone: the two branches have respectively N-S and E-W alignments, and both have the same dimensions: a 0.8 x 0.8 m^2 section, and a length of 8 m. The ditch is filled with exogenous topsoil, and thus has a higher magnetic susceptibility than the surrounding soil. Its resistivity contrast is low. EMI measurements were carried out in 1999 (Benech 2000), using three different devices: the MS2B magnetic susceptibility probe (Bartington, Ltd), the EM38 (Geonics ltd), which can in principle be used in both VCP and HCP configurations, and the SH3 (a laboratory prototype, (Parchas and Tabbagh 1978)). The MS2 has a 0.18m diameter coincident loop and thus a small depth of investigation, equal to approximately 0.1m, allowing the susceptibility determination to be restricted to the topsoil. The EM38 has a 1m coil separation and is operated at 14.6 kHz. The SH3 has a PARA coil orientation (the two coils have parallel axes at 35° from vertical so that their direct coupling is null in free space), a 1.5m coil separation, and is operated at 8.04 kHz. The dimensions of the studied area were 20x20 m^2, and this was surveyed using a 1 x1 m^2 measurement mesh. This mesh was however too coarse to allow changes in sign of the anomaly measured with the EM38 HCP configuration to be correctly monitored. All HCP data was thus excluded from the interpretation process. The measurements were carried out along North-South profiles, with the EM38 and SH3 being aligned with this profile (the line joining the transmitter to the receiver was parallel to the profile).

The three apparent magnetic susceptibility maps shown in Figure 2, and the two apparent resistivity maps shown in Figure 3, were processed by median filtering over a 3x3 points moving window. Even for the topsoil, the two branches of the ditch exhibit a greater magnetic susceptibility than the surrounding terrain, and the global shape of the feature can be recognized. In the apparent resistivity maps, the presence of the ditch is less well defined; it

appears to be slightly more resistive than the surrounding layer, and is clearly visible on the EM38-VCP map. However, the SH3 map reveals the natural variations of the medium, rather than those of the feature. This can be explained by the greater depth of investigation of this instrument. The apparent anisotropy effect associated (Guérin *et al.* 1996) with the configuration and orientation of the EM38-VCP may also have affected the measurements.

1D inversion results

In accordance with the electrical sounding carried out in the area nearby, the data were inverted by considering a three-layer ground comprising: a topsoil layer with 70 Ωm resistivity (14.3 mSm^{-1} conductivity), variable magnetic susceptibility, and 0.15 m thickness; a second layer having a variable resistivity and magnetic susceptibility and 1 m thickness; and a third layer, the sound limestone, having a resistivity of 300 Ωm (3.33 mSm^{-1}) and a magnetic susceptibility of 20 10^{-5} SI. The resistivity of the second layer, ρ_2, was first inverted using EM38-VCP and SH3 apparent resistivity data. Then, the topsoil and second layer magnetic susceptibilities, κ_{p1} and κ_{p2}, were inverted using the MS2B, EM38-VCP and SH3 apparent magnetic susceptibility data. The resulting maps are shown in Figures 2 and 3. As could be expected from the apparent resistivity maps, the exact shape of the ditch cannot be discerned on the ρ_2 map (Figure 2), but both branches appear to be more resistive, with apparent resistivity values reaching 100 Ωm (10 mSm^{-1}). As expected, in view of the instrument's shallow depth of investigation, the κ_{p1} map reproduces the MS2B map in shape and magnitude. The κ_{p2} map confirms the presence of a zone of significant magnetic contrast below the topsoil layer. All of the results reveal the inhomogeneity of both the material filled into the ditch, and the natural surrounding medium.

3D inversion results

The data inversion was applied over two small, separate targeted areas that are delineated by dotted rectangles in Figures 2 and 3. The values of contrast between the two

299 branches and the surrounding terrain, determined in terms of conductivity and magnetic
300 susceptibility, are summarized in Table 2.

301 When the data produced by the EM38-VCP and SH3 instruments are used in the
302 inversion, a conductivity contrast close to -10mSm^{-1} is obtained, corresponding to an absolute
303 resistivity of 100 Ωm (10 mSm^{-1}) for the ditch filling material, as opposed to about 50 Ωm
304 (20 mSm^{-1}) for the surrounding terrain. The computation time took 29 mn for the NS branch
305 and 32 mn for the EW one with a 4Go RAM and 2.5 GHz laptop computer.

306 When the inversion results are considered for each instrument separately, the contrasts
307 are very different: as could be expected from the apparent resistivity maps, the EM38-VCP
308 maps are comparable for the two branches and are characterised by a negative contrast (the
309 feature is less conductive); conversely, with the SH3 the contrast is positive (the feature looks
310 more conductive) but null and very low, and in fact the ditch is not detected. Thus, SH3
311 measurements do not contribute to the results of the two-instrument 3D inversion, which is
312 totally dominated by the data from the EM38-VCP.

313 When the magnetic susceptibility is considered, the values obtained for both branches
314 reveal a generally stronger magnetic feature. The absolute value of the ditch fill material lies
315 between 50 and 150 x 10^{-5} SI. Again, the results obtained with the EM38-VCP and SH3
316 instruments are significantly different in magnitude: with the EM38-VCP, the values of
317 contrast determined for the two branches are quite similar, whereas with the SH3 clearly
318 different results are found, approximately 40 x 10 $^{-5}$ SI for the N-S branch, and approximately
319 110 x 10^{-5}SI for the E-W branch. This difference remains difficult to explain, because the
320 anisotropy associated with the direction of the applied magnetic field is normally taken into
321 account in the 3D inversion process.

322 Globally, the experiment conducted over these artificial ditches shows that the
323 inversion results obtained with different instruments can be significantly different, and that

the coil configuration plays an important role in EMI instrument responses. In conclusion, it can be judicious to use several instrumental configurations when the depths of anomalous features are not known.

Field tests over two archaeological sites

Gallo-roman site of Vieil-Evreux (Eure, France)

The test was carried out in the *fanum* area of this site, called Gisacum during the Roman era. This is a religious centre, located 7 km east of the capital city of Aulerques Eburovices (now Evreux in Normandy) (Guyard and Lepert 1999). Several new surveying techniques and different devices (Flageul et al. 2013) have already been tested in this area, such that a series of control data was available. The soil resistivity was mapped using a three-depth multipole array ARP© (Automatic Resistivity Profiling) so that both the pattern of the different features and the resistivity ranges of the different materials are known. The site is located in the geological context of a flint-clay plateau, resulting from the weathering of the cretaceous chalk. Above this clay, which has a resistivity of approximately 15 Ωm, the archaeological remains have a variable thickness and can exceed 100 Ω.m in resistivity. In the *fanum* area, the thickness of the archaeological layer is approximately 90 cm. The tests were carried out using the DualEM 421S instrument, a multi-receiver EMI (DualEM sensor manual 2010) operated at 9 kHz. It associates one horizontal transmitter loop with three pairs of receivers. In each pair, the first receiver is horizontal, allowing HCP measurements to be made. By rotating the entire apparatus, VCP configuration measurements can be made. The second receiver of each pair is oriented in a radial direction from the transmitter, allowing PERP configuration measurements to be used. The receivers of the first pair are located at respectively 1m and 1.1m from the transmitter, those of the second pair at 2m and 2.1 m, and those of the third pair at 4m and 4.1m. However, in the present test data from the third pair

were not considered, and only HCP 1m, HCP 2m, PERP 1.1m and PERP 2.1m data was used for the 1D/3D inversion. The data was acquired at a high sampling rate, by towing the instrument (with a quad bike) 0.1m above the ground. Each data point was located using a dGPS system, thus allowing the resulting map to be produced on a fine, 0.3 x 0.3 m^2 mesh. The apparent resistivity maps obtained with the four configurations are shown in Fig. 4. The approximately 10m x 10m square *cella* can be seen at the centre of each of these images, and on the east and west sides the external walls of the *fanum*. The global apparent resistivity is found to have lower values with the PERP 2.1m and HCP 2m instrument configurations, than for shorter coil separations. This is due to the greater influence of the underlying flint-clay layer. In both HCP images, the anomalies generated by walls correspond to three parallel, resistive/conductive/resistive strips; this experimental result is in full agreement with the theory (Tabbagh 1986), and was achieved thanks to the fine mesh used for this survey. However, such anomalies with this coil configuration can lead to misinterpretation, if the experimental results are not compared with the theoretical model. The wall anomalies are more pronounced on the PERP 1.1m map than on the HCP 1m map, and the ability of the former to image the wall pattern appears to be equivalent to that of the electrical method (Dabas et al. 2015).

The 3D interpretation allows these different points to be more thoroughly investigated. To this aim, a limited 4.8 x 3.6 m^2 targeted area was defined, including the external wall , which is delineated by a rectangle in Fig. 5 (the *cella* itself appears to be more complicated, it probably has deeper underground sub-structures). In this zone, 3D interpretation of the electrical data acquired with the ARP© indicates that the wall has a section of 1.00 x 0.88 m^2 and a resistivity of 70.7 Ωm (14.1 mSm^{-1}), which is in contrast with the second, surrounding layer with a resistivity of 32 Ωm (31.2 mSm^{-1}). The conductivity contrast characterizing the wall is thus -17.1mSm^{-1}. Table 3 presents the conductivity contrast between the wall and

surrounding layer, computed using the same geometrical parameters (to define the wall's location and section), based on the data provided by each configuration alone, and on the combined data from all four configurations. In all cases, the contrast is found to be lower than that obtained with DC resistivity measurements. The conductivity contrast determined with the combined data is not greater than the contrast computed from the data produced by each individual instrument. The two configurations giving a qualitatively correct contrast, i.e. PERP 1.1m and HCP 2m, are those which also produce the clearest apparent resistivity maps. The near absence of contrast obtained with the PERP2 configuration, with no detection of the wall, can be explained by the depth of investigation of this configuration. The sign inversion obtained with the HCP 1m is a consequence of the three arched anomalies, and confirms that the use of a HCP configuration can lead to considerable interpretation difficulties in the case of small resistive features. These observations again emphasize the advantage and drawback associated with the simultaneous use of several configurations.

Neolithic enclosure at Balloy (Seine et Marne, France)

The study of this middle Neolithic enclosure provides an interesting example of the usefulness of 3D inversion. The eastern section of this 'Passy' type of funeral enclosure (Mordant 1997) has been the object of multi-method tests. This enclosure was detected by both electrical (square array of 1m side) and SH3 prospection, but not by magnetic prospection using a fluxgate gradiometer with 1nT sensitivity (Hesse 1987) and it is important to explain this failure. The apparent magnetic susceptibility map of this enclosure is shown in Fig. 5. On this site, the cultivated topsoil layer has a susceptibility of 100 x 10^{-5} SI, a resistivity of 70 Ωm and a thickness of 0.25 m. This layer covers a highly resistive gravel formation (300 Ωm) with a low susceptibility, equal to 20 x 10^{-5} SI.

3D interpretation was applied to a targeted area in which the ditch can be clearly distinguished (see contours in Figure 5). It shows that the ditch fill material, which contrasts

with the gravel, is thin, i.e. has a section of 1.4 x 0.4 m^2, and has a relatively low magnetic susceptibility of 51 x 10^{-5} SI. Using these parameters, the magnetic anomaly determined with a fluxgate vertical gradient is not more than 0.5 nT/m. Both the limited thickness and the limited contrast explain why no magnetic anomaly was observed, even with the addition of viscous magnetic remanent magnetization, and confirm the usefulness of EM susceptibility measurements over thin features.

Conclusion

1D interpretation allows underground structures to be more clearly delineated, and permits a better assessment of variations in the soil's physical properties than simple mapping of apparent properties. The complementary 3D inversion allows solving a series of issues: correction for the apparent anisotropy generated by the instrument configuration, multi-arched anomalies, precise location of lateral changes and determination of the contrasts between the considered body and its surrounding medium.

When applied to EMI data, the rapid 1D/3D inversion process we have proposed not only allows an (expected) improvement in interpretation to be achieved, but also emphasizes the importance of the instrument's geometry, which should be optimally matched with the objectives of the survey. This inversion process is shown to be useful for the assessment of multi-configuration instrument capabilities. In particular, it confirms the difficulties encountered with the use of an HCP configuration, and the conclusions of early theoretical studies of this technique.

Since the analytical and numerical (MoM) calculation method presented in this study is the same as the one already used with the DC resistivity technique, 1D/3D inversion will offer the possibility of combining DC and EMI data in a joint inversion. This would be useful

423 to surveyors because EMI is faster for in-field mapping, while DC is more reliable for the
424 determination of electrical resistivity contrasts of resistive features.

425 Although interpretations of both electrical conductivity and magnetic susceptibility
426 measurements are presented in this study, it is important to note that contrary to the electrical
427 resistivity which most often belongs to the [1, 10,000 Ωm] interval, the range of relative
428 magnetic permeability values is very narrow: between 1.00 and 1.01. Consequently it is
429 sufficiently small for the 'magnetic' EMI responses to be considered as linear. This means
430 that a wide range of linear techniques, such as linear filtering, can be applied to the
431 interpretation of apparent magnetic susceptibility maps. Further research is needed, to
432 evaluate potential developments and applications for these techniques.

433

434

435 **References**

436 Auken E. and A. V. Christiansen, 2004, Layered and laterally constrained 2D inversion of
437 resistivity data: Geophysics, **69**, 752-761.

438 Bendjoudi H., P. Weng, R. Guérin and J. F. Pastre, 2002, Riparian wetlands of the middle
439 search of the Seine river (France): historical development, investigation and present
440 hydrologic functioning: Journal of Hydrology, **263**, 131-155.

441 Benech C., 2000, Interprétation conjointe de cartographies magnétique et électromagnétique
442 des propriétés magnétiques des sols anthropisés. Thèse Université Pierre et Marie Curie,
443 Paris.

444 Benech C., A. Tabbagh and G. Desvignes, 2002, Joint interpretation of E. M. and magnetic
445 data for near-surface studies*:* Geophysics, **67**, 1729-1739.

446 Brinon C., F.-X. Simon, and A. Tabbagh, 2012, Rapid 1D/3D inversion of shallow resistivity
447 multipole data: examples in archaeological prospection: Geophysics, **77**, no. 3, E193-E201.

448 Bonsall J., R. Fry, C. Gaffney, I. Armit, A. Beck and V. Gaffney, 2013, Assessment of the
449 CMD mini-explorer, a new low-frequency multi-coil electromagnetic device, for
450 archaeological investigations: Archaeological Prospection, **20**, 219-231.

451 Dabas M., A. Anest, J. Thiesson and A. Tabbagh, 2015, Slingram EMI devices for
452 characterizing resistive features using apparent conductivity measurements: check of the
453 DualEM-421S instrument and field tests: Submitted to Archaeological Prospection.

454 De Jong E., A. K. Ballantyne, D. R. Cameron and D. W. L. Read, 1979, Measurement of
455 apparent electrical conductivity of soil by an electromagnetic induction probe to aid salinity
456 surveys: Soil Science Society of America Journal, **43**, 810-812.

457 DualEM-421S User's manual, 2010, Milton, Ontario, Canada, 32p.

458 Farquharson C. G., D. W. Oldenburg and P. S. Routh, 2003, Simultaneous 1D inversion of
459 loop–loop electromagnetic data for magnetic susceptibility and electrical conductivity:
460 Geophysics: **68**, 1857-1869.
461 Flageul S., M. Dabas, J. Thiesson, F. Réjiba and A. Tabbagh, 2013, First in situ tests of a new
462 electrostatic resistivity meter: Near Surface Geophysics, **11**, 265-273.
463 Guérin R., Y. Méhéni, G. Rakontodrasoa and A. Tabbagh, 1996, Interpretation of Slingram
464 conductivity mapping in near surface geophysics: using a single parameter fitting with 1D
465 model: Geophysical Prospecting, **44**, 233-249.
466 Guyard L. and T. Lepert, 1999, Le Vieil- Evreux, ville sanctuaire gallo-romaine : Archeologia
467 **359**, 20-29.
468 Hesse A., 1987, Balloy 1986-1987. Rapport de synthèse sur les prospections géophysiques
469 des vestiges archéologiques : Direction régionale des antiquités d'Ile de France, août 1987,
470 15p.
471 Hoefer G., J. Bachmann and K. H. Hartge, 2010, Can EM38 probe detect spatial pattern of
472 subsoil compaction?, In Proximal Soil Sensing, Progress in Soil Science 1, R.A. Viscarra
473 Rossel et al. (eds.), Chapter 22, 265-273.
474 Hohmann G. W., 1975, Three dimensional induced polarization and electromagnetic
475 modeling: Geophysics, **40**, 309-320.
476 Huang H. and D. C. Fraser, 1996, The differential parameter method for multi-frequency
477 airborne resistivity mapping: Geophysics, **61**, 100-109.
478 Huang H. and D. C. Fraser, 2002, Dielectric permittivity and resistivity mapping using high
479 frequency, helicopter born EM data: Geophysics, **67**, 727-738.
480 Kacahnoski R. G., E. G. Gregorich and I. J. van Wesenbeek, 1988, Estimating spatial
481 variations of soil water content using non-contacting electromagnetic inductive methods:
482 Canadian Journal of Soil Science, **68**, 715-722.

Marquardt, D. W., 1963, An algorithm for least square estimation of nonlinear parameters: Journal of the Society for Industrial and Applied Mathematics, **11**, 431–441.

McNeill J. D., 1980, Electromagnetic terrain conductivity measurement at low induction numbers: Geonics Limited Technical Notes, **TN-6**, 15p.

Mordant D., 1997, Le complexe des Réaudins à Balloy: enceinte et nécropole monumentale. La Culture de Cerny. Nouvelle économie, nouvelle société au Néolithique : Actes du Colloque International de Nemours 1994, Mémoires du Musée de Préhistoire d'Ile-de-France, **6**, 449-479.

Parchas C. and A. Tabbagh; 1978, Simultaneous measurement of electrical conductivity and magnetic susceptibility of ground in electromagnetic prospecting: Archaeo-Physika, **10**, 682-691

Raiche A. P., 1974, An integral equation approach to three dimensional modelling: Geophysical Journal of the Royal Astronomical Society, **36**, 363-376.

Saey T., P. De Smedt, E. Meerschman, M.-M. Islam, F. Meeuws, E. van De Vijver, A. Lehouck and M. van Meirvenne, 2012, Electrical conductivity depth modelling with a multi-receiver EMI sensor for prospecting archaeological features: Archaeological Prospection, **19**, 21-30.

Santos, F. M., 2004, 1-D laterally constrained inversion of EM34 profiling data: Journal of Applied Geophysics, 56, 123–134.

Scollar I., A. Tabbagh, A. Hesseand I. Herzog, 1990, Archaeological prospection and remote sensing. Cambridge University Press, 674p.

Tabbagh A., 1985, The response of a tree dimensional magnetic and conductive body in shallow depth EM prospecting: Geophysical Journal of the Royal Astronomical Society, **81**, 215-230.

507 Tabbagh A., 1986, What is the best coil orientation in the slingram electromagnetic
508 prospecting method? Archaeometry, **28**, 185-196.
509 Thiesson J, M. Dabas and S. Flageul, 2009, Detection of resistive features using towed
510 Slingram electromagnetic induction instruments: Archaeological Prospection, **16**: 103-109.
511 Tite M. S. and C. E. Mullins, 1970, Electromagnetic prospecting on archaeological sites using
512 a soil conductivity meter: Archaeometry, **12**, 97-106.
513 Vitharana U. W. A., M. van Meirvenne, D. Simpson, L. Cockx and G. Hofman, 2008,
514 Agronomic consequences of potential zones delineated on the basis of EM38DD
515 measurements: Near Surface Geophysics, **6**, 289-296.
516

Figure captions

Figure 1: Synthetic data for three different Slingram devices, recorded above an elongated, 3D body (resistivity = 20 Ωm, susceptibility = 80 x 10^{-5} SI) of dimensions: length=3 m, width=1m, thickness=1 m, embedded in the second layer of a three layer ground, the top of which is located 0.3 m below the ground surface (first layer 100 Ωm, 30 x 10^{-5} SI and 0.2m, second layer 200 Ωm, 20 x 10^{-5} SI and 2m, third layer 50 Ωm and 10 x 10^{-5} SI). The rectangular dotted line indicates the contours of the targeted area used for 3D interpretation

(a) Apparent resistivity maps for in-line

(b) Apparent magnetic susceptibility maps for in-line measurements, and vertical section of the feature.

Figure 2: Apparent magnetic susceptibility maps of the artificial L-shaped feature at the Garchy site and first and second layer susceptibility variations after 1D inversion. The two dashed rectangles indicate the contours of the two targeted areas used for 3D inversion.

Figure 3: Apparent resistivity maps of the artificial L-shaped feature at the Garchy site and second layer resistivity variations after 1D inversion

Figure 4: Apparent resistivity maps of the Fanum area at Vieil-Evreux, corresponding to quadrature measurements using DualEM HCP 1m, HCP 2m, PERP1.1m and PERP2.1m configurations. The rectangles indicate the contour of the targeted area on which 3D interpretation is applied.

Figure 5: Apparent magnetic susceptibility map of the Neolithic funeral enclosure at Balloy (Seine et Marne, France), using in-phase SH3 measurements. The rectangles indicate the contour of the targeted area used for 3D inversion.

Table captions

Table 1: Numerical values obtained after 3D inversion of synthetic data. First four columns: resistivity, conductivity and vertical extent of the body and relative RMS error, based on apparent resistivity data inversion. Last three columns: magnetic susceptibility, vertical extent of the body, and relative RMS error based on apparent magnetic susceptibility inversion. The definition of the relative RMS error is the following: $RMS = \sqrt{\frac{1}{N_{app}N_{point}} \sum_{i=1}^{N_{app}} \sum_{j=1}^{N_{point}} \left(\frac{M_{i,j} - R_{i,j}}{R_{i,j}} \right)^2}$ where N_{app} is the number of apparatus, N_{point} the number of points, $M_{i,j}$ the measurement with the i apparatus at the point j and $R_{i,j}$ the theoretical measurement with the i apparatus at point j.

Table 2: Electrical conductivity and magnetic susceptibility contrasts and inversion relative RMS error obtained from 3D inversion, using each instrument separately, and using both instruments together. The starting a priori values adopted for conductivity are indicated in parentheses.

Table 3: Conductivity contrasts and inversion relative RMS error obtained between the external *fanum* wall and the surrounding layer (the wall has a 1.00 x 0.88 m^2 section and is centred at 0.70m depth). The starting a priori values adopted for conductivity are also indicated.

563

564

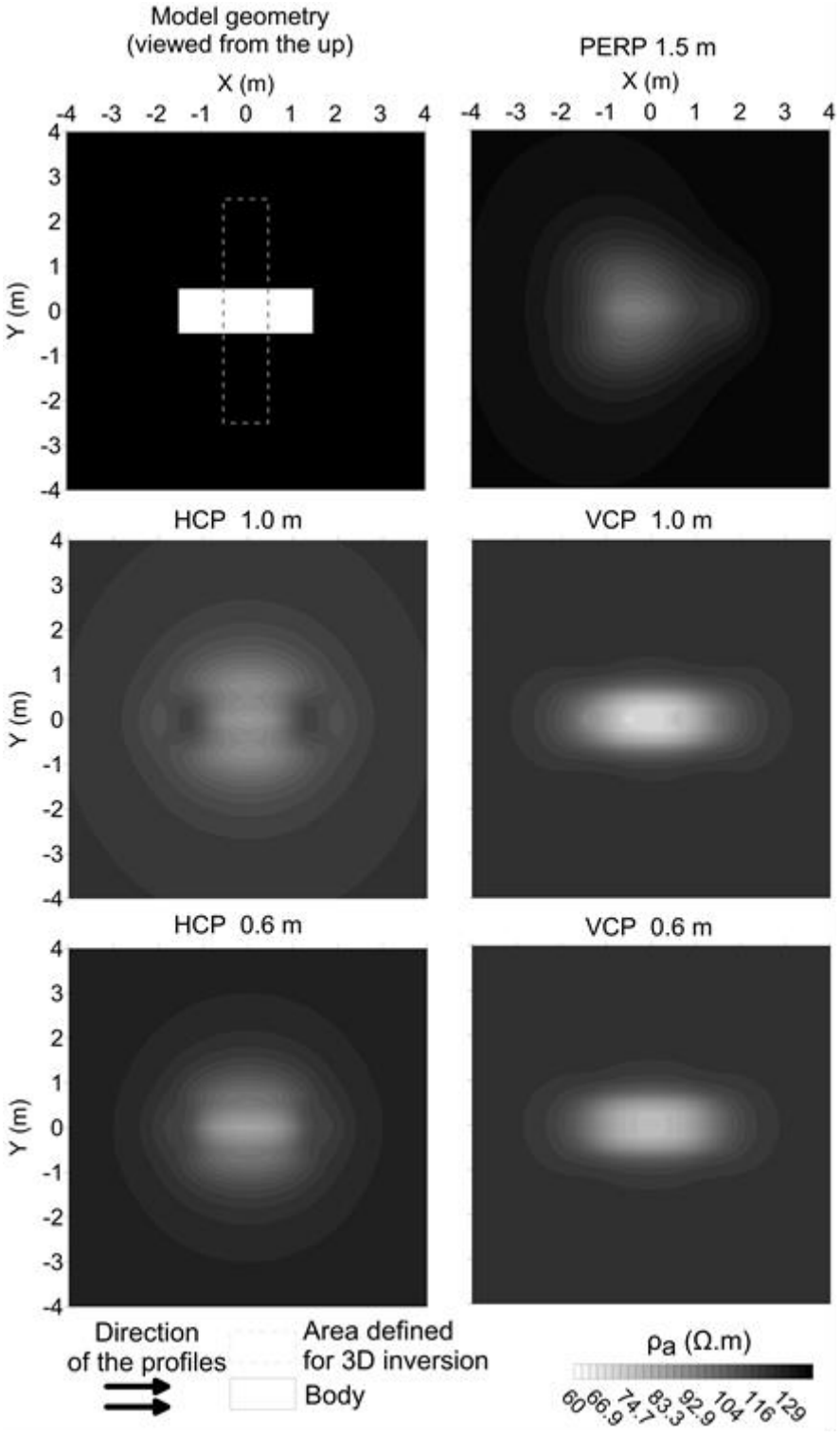

565

566 Fig. 1a

567

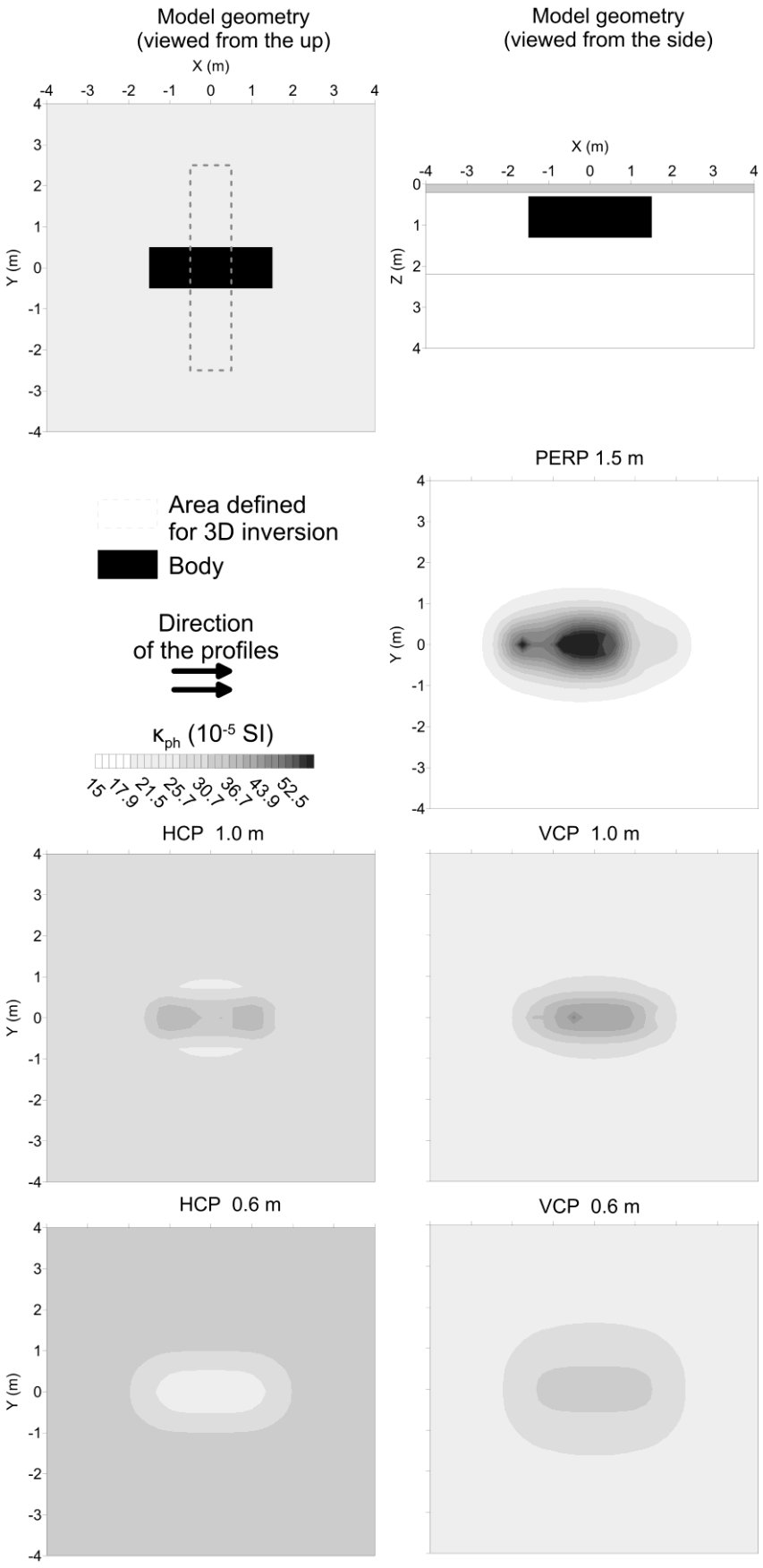
Model geometry
(viewed from the up)
X (m)
Y (m)
Model geometry
(viewed from the side)
X (m)
Z (m)
Area defined
for 3D inversion
Body
Direction
of the profiles
κph (10-5 SI)
15 17.9 21.5 25.7 30.7 36.7 43.9 52.5
PERP 1.5 m
HCP 1.0 m
VCP 1.0 m
HCP 0.6 m
VCP 0.6 m

Fig. 1b

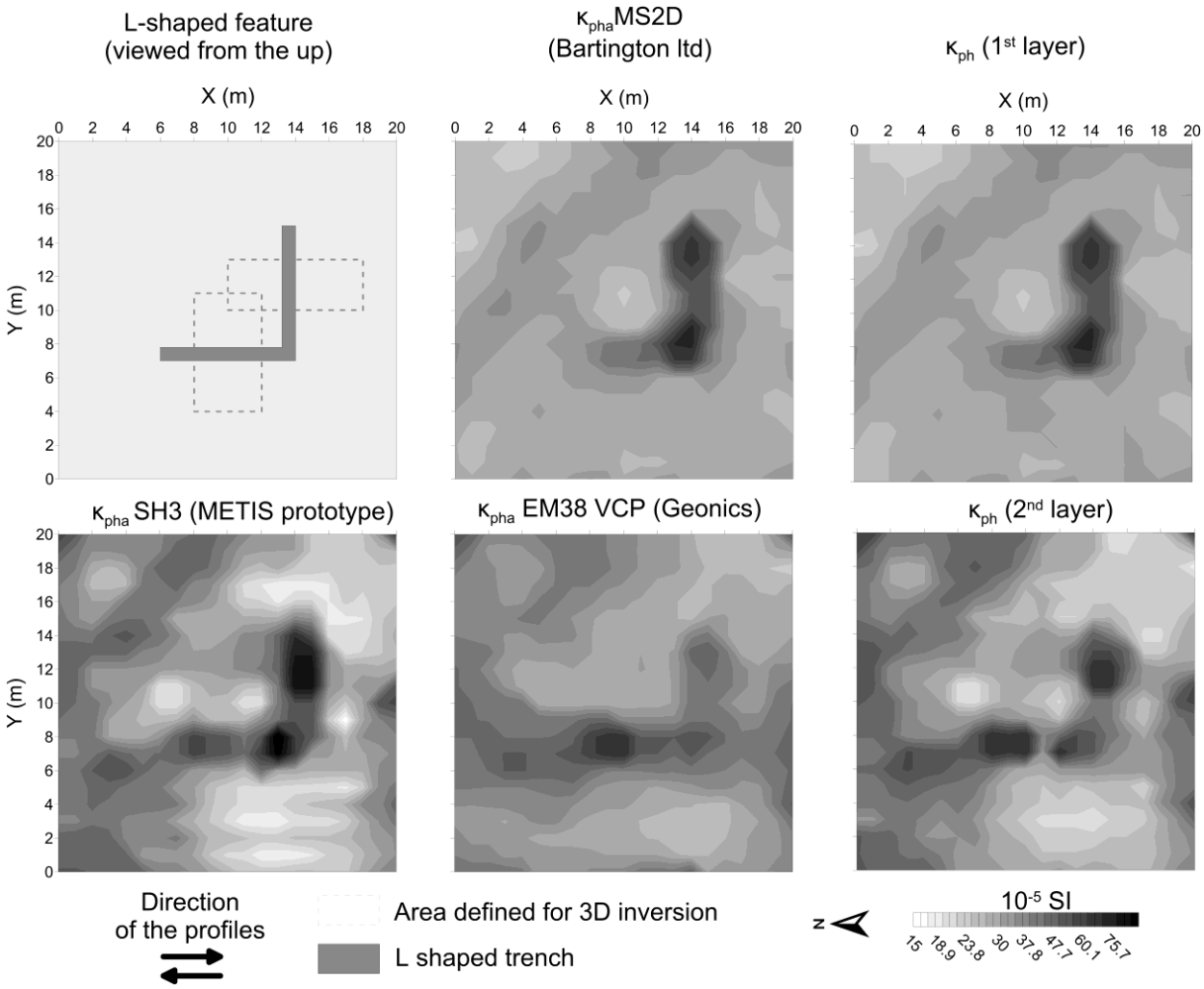

570

571 Fig. 2

572

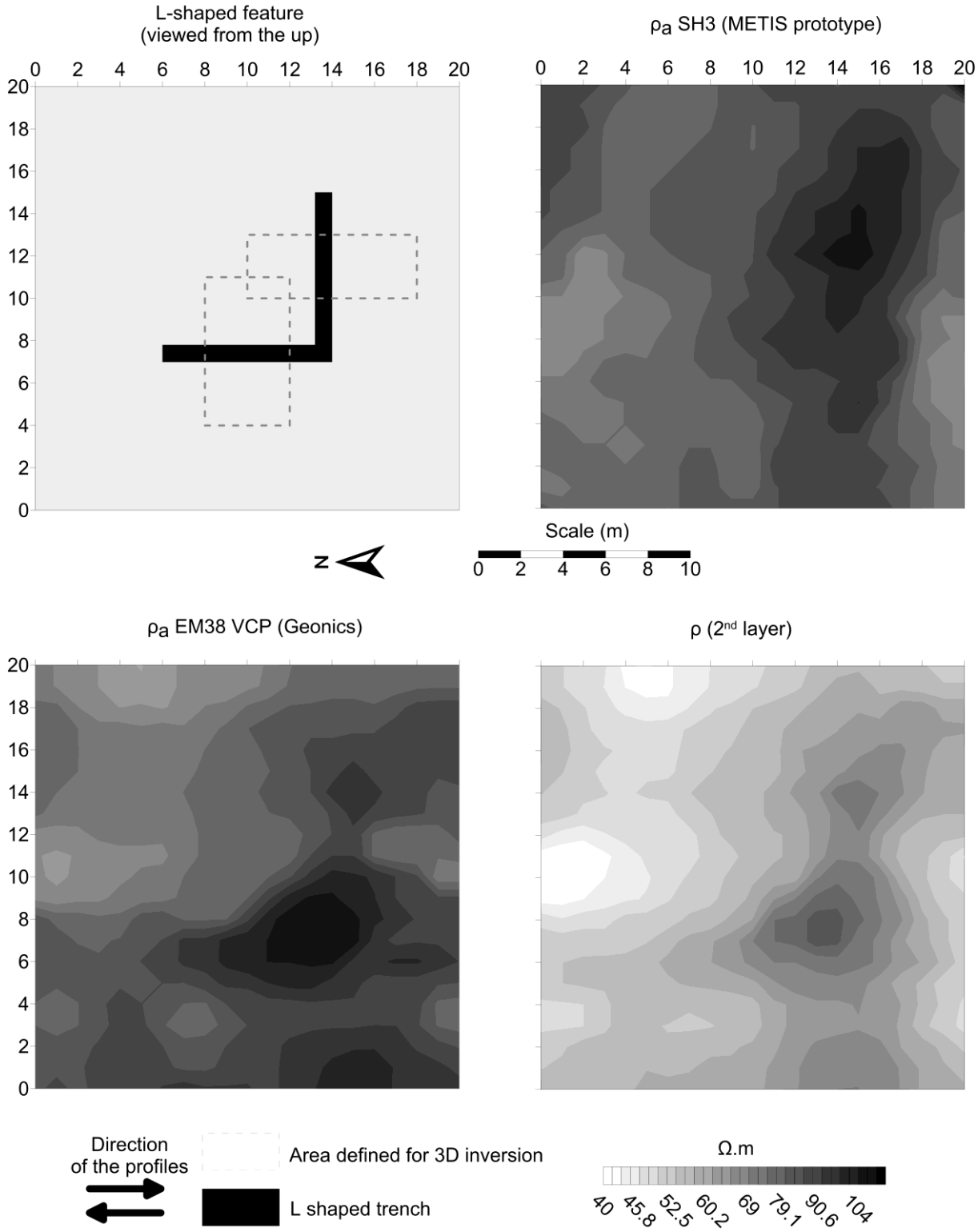

573

574

575 Fig. 3

576

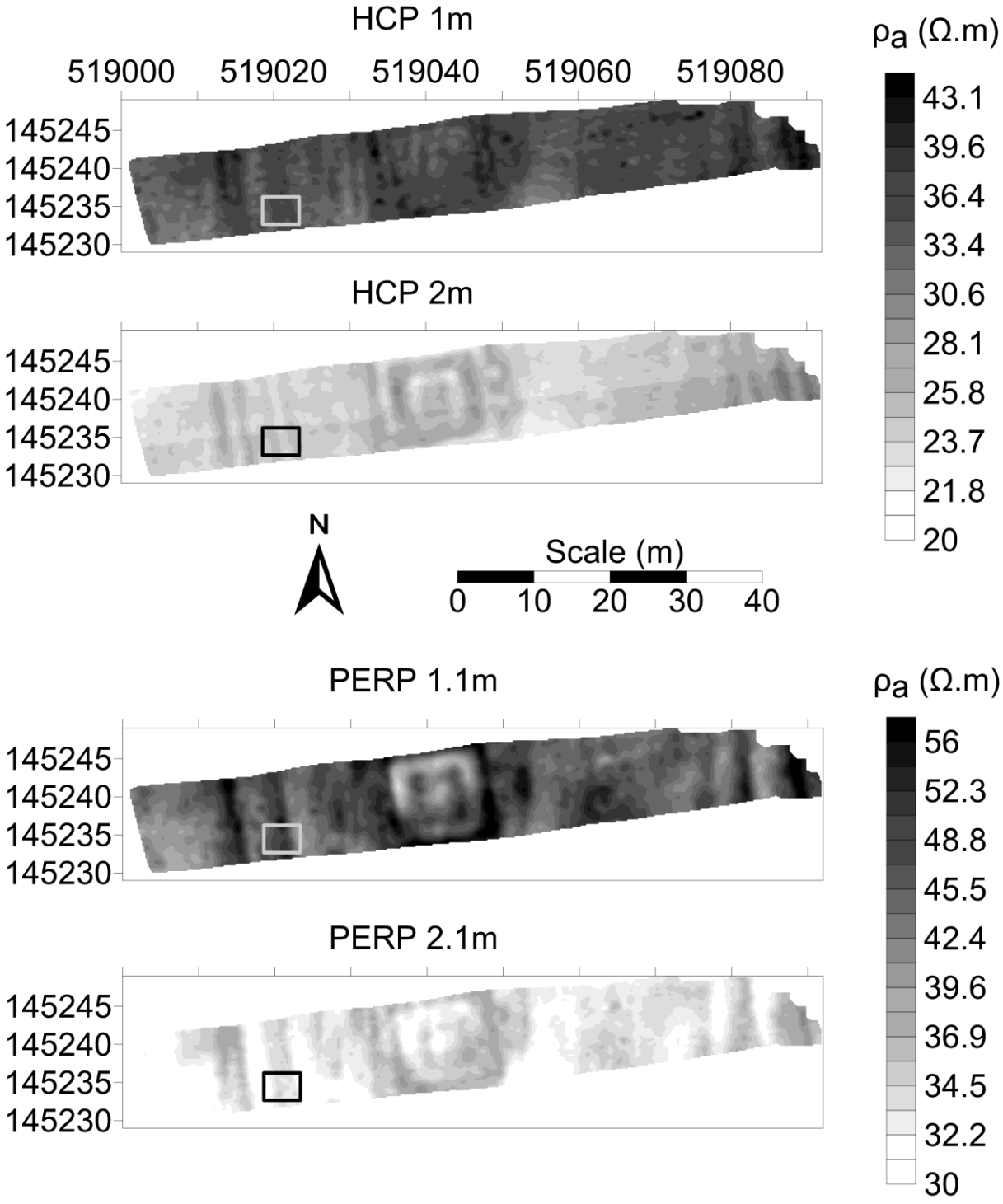

577

578 Fig. 4

579

580

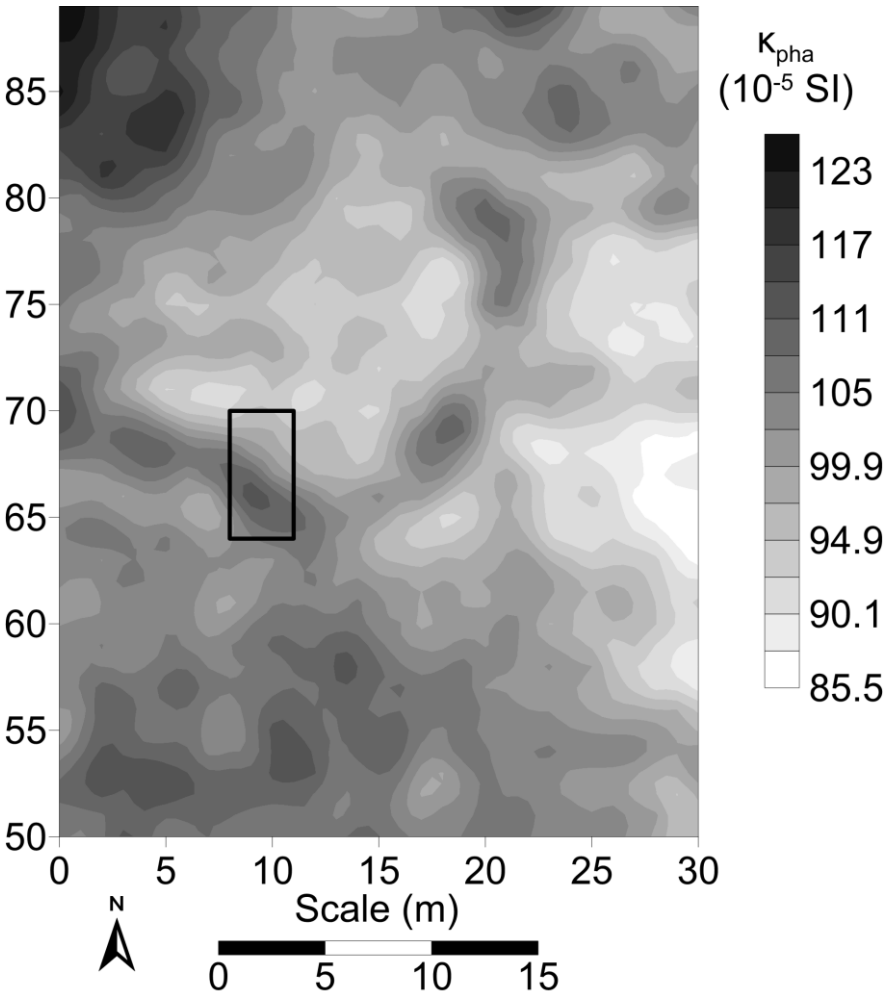

581

582 Fig. 5

583

584

585

	ρ_b (20 Ωm)	σ_b (50 mSm^{-1})	Zl (1m) Using the resistivity map	Relative RMS error	κ_b (80 10^{-5} SI)	Zl (1m) Using the susceptibility map	Relative RMS error	κ_b (80 10^{-5} SI)
VCP 0.6 m	20.9	47.8	0.84	0.028	76.5	0.98	0.030	76.5
HCP 0.6 m	22.3	44.8	0.82	0.021	77.5	0.95	0.094	77.5
VCP 1 m	19.4	51.5	0.85	0.038	80.1	1.00	0.031	80.1
HCP 1 m	22.9	43.7	0.80	0.034	66.8	0.96	0.056	66.8
PERP 1.5 m	23.5	42.6	0.81	0.043	81.3	1.02	0.059	81.3
5 configurations	21.4	46.7	0.82	0.039	79.8	0.98	0.036	79.8

586 Table 1

587

588

	N-S Branch		E-W Branch	
	Electrical conductivity contrast (in mSm^{-1}) with starting a priori value	Relative RMS error	Electrical conductivity contrast (in mSm^{-1}) with starting a priori value	Relative RMS error
EM38-VCP (Quadrature)	-10.0 (a priori at -6.2)	0.126	-13.9 (a priori at -6.2)	0.071
SH3 (Quadrature)	0.0 (a priori at -14.9)	0.058	1.75 (a priori at -12.0)	0.092
EM38-VCP & SH3 (Quadrature)	-8.4 (a priori at -9.0)	0.102	-9.6 (a priori at -8.6)	0.097
	Magnetic susceptibility contrast (in 10^{-5} SI)		Magnetic susceptibility contrast(in 10^{-5} SI)	
EM38-VCP (in-Phase)	64.5	0.076	50.5	0.170
SH3 (in-Phase)	39.5	0.140	108.5	0.150
EM38-VCP & SH3 (in-Phase)	47.4	0.077	109.7	0.084

589 Table 2

590

591

592

	Conductivity contrast starting a priori values (in mSm^{-1})	Inverted conductivity contrast (in mSm^{-1})	Relative RMS error
HCP 1m + HCP 2m + PERP 1.1m +PERP 2.1m	-23.3	-0.32	0.021
HCP 1m	-28.5	+10.5	0.003
HCP 2m	-30.8	-3.5	0.002
PERP 1.1m	-28.5	-8.0	0.005
PERP 2.1m	-28.5	0.34	0.002

593 Table 3

594